Boosting Circularly Polarized Luminescence from Alkyl-Locked Axial Chirality Scaffold by Restriction of Molecular Motions

*Wenbin Huang, Kang Zhou, Engui Zhao, and Zikai He**

W. Huang, E. Zhao, Z. He
School of Science, Harbin Institute of Technology, Shenzhen, 518055, China
E-mail: hezikai@hit.edu.cn

K. Zhou
Hoffman Institute of Advanced Materials, Shenzhen Polytechnic, Shenzhen, 518055, China

Keywords: Bidibenzo[*b*,*d*]furan, Circularly-Polarized Luminescence, Locked Axial Chirality, Room-Temperature Phosphorescence, Restriction of Molecular Motions

Boosting the circularly polarized luminescence of small organic molecules has been a stubborn challenge because of weak structure rigidity and dynamic molecular motions. To investigate and eliminate these factors, here, we carried out the structure-property relationship studies on a newly-developed axial chiral scaffold of bidibenzo[*b*,*d*]furan. The molecular rigidity was finely tuned by gradually reducing the alkyl-chain length. The environmental factors were considered in solution, crystal, and polymer matrix at different temperatures. As a result, a significant amplification of the dissymmetry factor g_{lum} from 10^{-4} to 10^{-1} with a 146-fold magnification was achieved, corresponding to the situation from (R)-4C in solution to (R)-1C in polymer film at room temperature. A synergistic strategy of increasing the intramolecular rigidity and enhancing the intermolecular interaction to restrict the molecular motions was thus proposed to improve circularly polarized luminescence. The though-out demonstrated relationship will be of great importance for the development of high-performance small organic chiroptical systems in the future.

1. Introduction

Recently, circularly polarized luminescence (CPL) materials have found versatile potential applications in intelligent sensing, three-dimensional display, optical information storage, organic light-emitting diode, biological imaging, etc.[1-3] Significant attention has been received together with their fascinating photophysical characteristics.

Currently, two-type methodologies can generate interesting CPL. One is the physical optical conversion, where emitting light is passed through a linearly polarized plate and a quarter-wave plate in succession; the other is the direct light emission from chiral systems[4]. Obviously, the former method causes severe light loss and is detrimental to developing high-performance CPL, compared to the energy-efficiency latter one. Moreover, the later can introduce additional functionalities, such as stimuli-responsive behavior[5-9], delayed fluorescence[10, 11], room-temperature phosphorescence[5, 6, 12-17], chirality inversion[18-20], solvent-dependent chirality transfer[21], wavelength regulation[22-24], waveguide laser[25], mechanochromic luminescence[26], and so on[27, 28]. Thus, various organic CPL systems have been developed including nanodots[29, 30], organometallic complexes[31, 32], self-assembly systems[33, 34], small organic molecules[35-39], π-conjugated polymers[40-42], chiral-photonic or liquid crystals[43, 44].

Among them, purely organic and chiral small molecules become the favour of academic interests for their advantages of facile preparation, structural tuneability, precise chirality control, and good biocompatibility. However, limited by the small chirality, aggregation-caused quenching, and dynamic molecular motions, it is quite difficult to obtain satisfactory CPL performance for pure organic and chiral small molecules in terms of unnoticeable polarization factor, low quantum yield, and crude-controlled lifetime. Hence, it is of great importance to explore novel chiral emissive scaffolds and to develop a rational design strategy for boosting circularly polarized luminescence.

Restriction of intramolecular motions has been recognized as the general mechanism for interpreting the aggregation-induced emission phenomena and thus remarkably promotes the development of the area[45, 46]. Here, we extend the scope to the restriction of molecular motion, including internal structure rigidification and external molecular interactions. It can stabilize both the excited state and chiral configuration to enhance the CPL performance by reducing nonradiative dissipation pathways and dynamic reorganization of the excited chiral states[47]. According to earlier reports, CPL can indeed be tuned by intramolecular rigidity, environmental confinement, and cryogenic condition. For example, Mazaki et al. found that tethering cyclic binaphthyl framework can suppress structural relaxation to improve CPL[48]. Zhao et al. discovered chain-length dependent circular dichroism and aggregation-induced CPL[49]. The amplification of chiroptical performance by rigidifying molecular configuration has been well investigated by Zheng and Liu[50-54]. Tadashi Ema also demonstrated that CPL enhancement can be accomplished by converting flexible excimer into rigid excimer[55]. There are even more

excellent strategies of regulating aggregate state to enhance the CPL by self-assembly, liquid crystal, metal-organic framework, polymer matrix, crystallization, supramolecular encapsulation, and chiral cage.[56-60] These results further confirm that CPL enhancement can be achieved by increasing rigidity and enhancing interactions. However, a systematic and comprehensive demonstration of the structure-property relationship between the restriction of molecular motions and the enhancement of CPL performance is still lacking.

Herein, we choose a newly-developed axial chiral scaffold of bidibenzo[*b*,*d*]furan for its facile synthesis and easy chiral resolution. As shown in Scheme 1, the axial chirality is gradually rigidified by manipulating the length of the locking alkyl chain. The environmental rigidity also varies from solution to crystal and to the polymer matrix and is tuned at different temperatures. By employing the strategy of increasing intramolecular rigidity and enhancing environmental confinement, great enhancement of dissymmetry factor ($|g_{lum}|$) and a positive correlation between the $|g_{lum}|$ and the extent of restriction of molecular motions were found, giving a 146-fold amplification from 10^{-4} to 10^{-1} level. A rational and effective structure-property relationship was carefully demonstrated as the synergistic effect of restriction of molecular motions can remarkably boost the CPL performance on an alkyl-locked axial chirality scaffold.

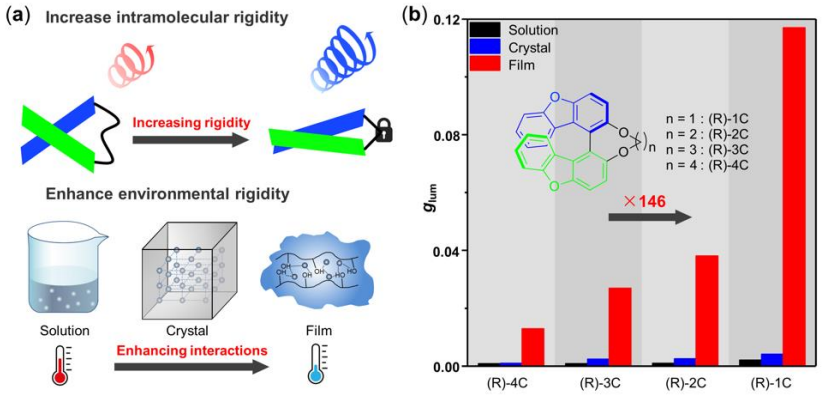

Scheme 1. (a) Strategies for boosting circularly polarized luminescence by increasing intramolecular rigidity and enhancing intermolecular interactions. (b) The magnitude enhancement of $|g_{lum}|$ from (R)-4C to (R)-1C in solution, crystal, and film at room temperature.

2. Results and Discussion

Target compounds with different alkyl linkers were designed and prepared following the procedures as shown in Scheme 2. The bidibenzo[*b*,*d*]furan scaffold (R/S)-OMe was firstly constructed through multi-step reactions, including halogenation, alkoxy group protection, and C-C coupling[61]. Different alkyl-locked enantiomers were then synthesized through simple de-protection, NHC-catalysed kinetic resolution[62], and

alkylation reactions (For details, see Scheme S1). The structures are detailedly characterized by ^{1}H and ^{13}C NMR spectrometry (Charts S1-S7), high-resolution mass spectrometry, and chiral high-performance liquid chromatography (Chart S8). The enantiomeric excess (*ee*) values are estimated as high as 99.9% *ee* for R isomers and 96.5% *ee* for S isomers. The chiral scaffolds are found robust, and no racemization behaviours are observed during the investigation processes. 2-OMeDBF and (R/S)-OMe are also included as references for optical spectra and molecular structure comparison.

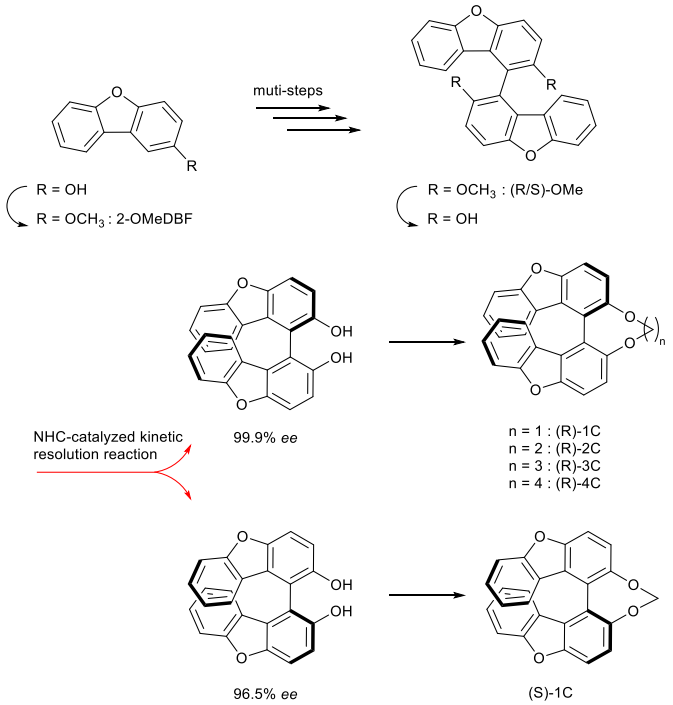

Scheme 2. The synthetic route and molecular structures of (R)-1C, (R)-2C, (R)-3C, (R)-4C, (S)-1C, 2-OMeDBF, and (R/S)-OMe.

Single-crystals of these compounds were successfully obtained by slow solvent evaporation and subjected to single-crystal X-ray diffraction analysis, from which their absolute conformations and molecular structures were determined[63]. To compare their structures in the free state, we applied density-functional theory to simulate molecular structure at the ground state. As summarized in Figure 1, the dihedral angle of uncyclized (R/S)-OMe is close to orthogonal and indeed larger than those of cyclized (R)-analogues. The dihedral angles of molecular structure in (R)-analogues correspondingly decrease with the reduction of the locking chain. A similar trend is observed from calculated structures, lowering from 102° to 58°. These results are understandable and predictable because the short alkyl chain locks the twisting of bidibenzo[*b,d*]furan scaffold and causes resulting intermolecular constraint. There are still some differences between experimental and simulated configurations, which should attribute to molecular

interactions in crystal packing and lead to the compression of dihedral angles. It is noted that the four methylene groups in (R)-4C cause an unexpected decrease in dihedral angle due to the allowed twisting freedom from a longer alkyl chain. So, it is not true that (R)-4C is more constrained. Moreover, pure enantiomeric molecules of (S)-1C, (R)-1C, (R)-2C, (R)-3C, and (R)-4C all pack in chiral space groups and verify their absolute axial conformations in single crystals with close to zero Flack factors (see Tables S1-S6 and supporting cif files). Besides, the perfect mirrored pair of (S)-1C and (R)-1C was found in both crystal and calculated structures.

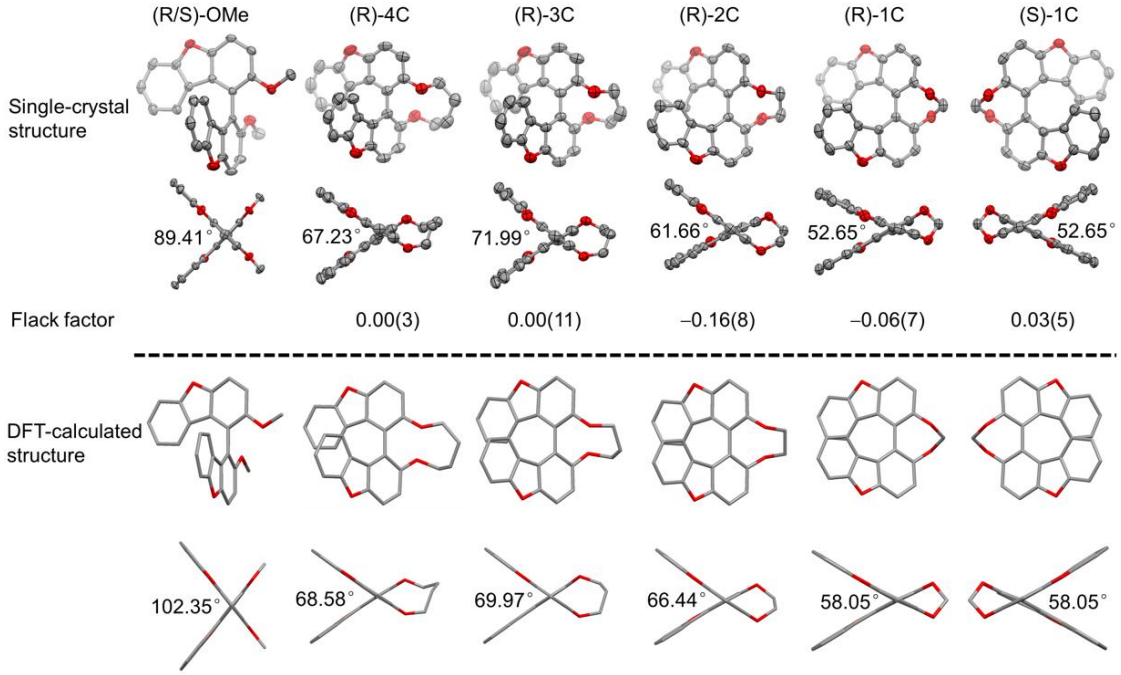

Figure 1. Single-crystal structures (ellipsoid with 50% probability and hydrogen atoms are omitted for clarity) and density-functional theory optimized structures (capped sticks with hydrogen atoms omitted for clarity) of (R/S)-OMe, (R)-4C, (R)-3C, (R)-2C, (R)-1C, and (S)-1C at b3lyp/6-311g(d,p) level.

The decrease in dihedral angle is conducive to increasing both π conjugation and intramolecular rigidity. To gain deeper insight, photophysical properties of unimolecular (R)-1C, (R)-2C, (R)-3C, (R)-4C, (S)-1C, 2-OMeDBF and (R/S)-OMe were then investigated in solutions. As shown in Figure 2a, the basic absorption range of these molecules covers a similar UV region of 260 nm to 360 nm, indicating the poor overall conjugation of the axial skeleton. But it is found the absorption edge exhibits a slight redshift from 2-OMeDBF to (R/S)-OMe and locked enantiomers. It reflects the subtle variation among these analogues, originating from the reduced dihedral angle and molecular flexibility. In detail, the absorption band at 320-360 nm is corresponding to

the first singlet excited state (S_1), which attributes to the whole conjugated π orbitals of molecules. So, the redshifted absorption edge indicates the increase of molecular conjugation. (R)-4C and (R/S)-OMe have relatively longer absorption wavelengths because they endow higher molecular flexibility and more accessible planar configurations (small dihedral angle). However, the molar extinction coefficient (ε) gets significantly reduced because the high molecular flexibility causes poor Frank-Condon factors due to molecular motions.[64] As a result, (R)/(S)-1C has considerable absorption wavelength but the strongest molar extinction coefficient, implying good π conjugation and the best molecular rigidification. Besides, as the dihedral angle increases, the absorption bands at 275-300 nm enhance, indicating that the degree of segmental conjugation increases and the degree of whole molecular conjugation decreases. The calculated HOMOs, LUMOs, and energy gaps also show a consistent trend; that is, the reduction of the dihedral angle leads to the increase of conjugation with lower energy levels of frontier orbitals and small energy gaps (Figure S1).

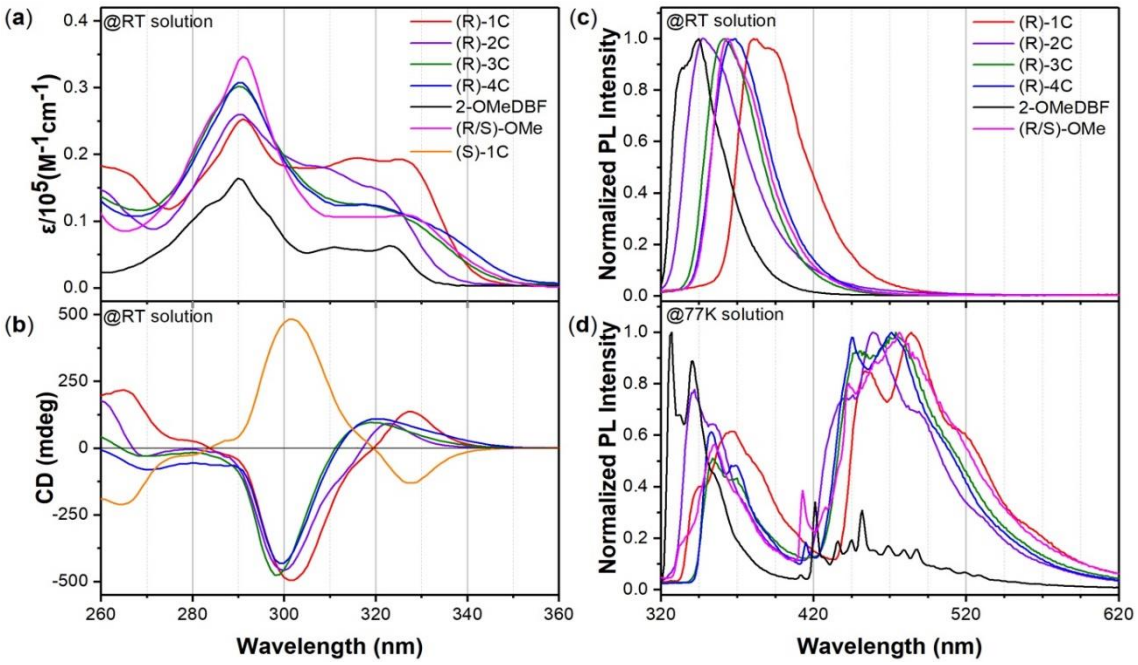

Figure 2. (a) UV-Visible absorption spectra, (b) circular dichroism spectra (10^{-4} M in 2-methyltetrahydrofuran), (c) normalized room-temperature photoluminescence spectra, and (d) normalized photoluminescence spectra at 77 K of (R)-1C, (R)-2C, (R)-3C, (R)-4C, (S)-1C, 2-OMeDBF and (R/S)-OMe in 2-methyltetrahydrofuran (10^{-5} M).

We then further investigated their fluorescence properties. Shown in Figure 2c and 2d, it can be observed that as the dihedral angle was decreased (from (R/S)-OMe, to (R)-4C, then to (R)-1C), their emission was generally redshifted, demonstrative of the increase of conjugation in their excited states. Among them, (R)-2C exhibited blue-

shifted emission, suggestive of its reduced degree of conjugation in the excited state (Figure 2c). This might be ascribed to the ring strain-induced larger dihedral angle in the excited state. When the temperature was lowered to 77 K, these molecules exhibited significant phosphorescence (Figure S2 and Table S7). As shown in Figure 2d, photoluminescence (PL) spectra in 2-methyltetrahydrofuran solutions at 77 K showed a distinct vibrational phosphorescence band at 410-620 nm, in addition to the fluorescence at short wavelength. As the dihedral angle was decreased, phosphorescence was gradually redshifted. Compared with 2-OMeDBF, the phosphorescence of alkyl-locked molecules was obviously enhanced, as suggested by their increased phosphorescence-to-fluorescence ratio. In general, the ratio of phosphorescence to fluorescence and the lifetime of luminescence reflected the efficiency of the intersystem crossing process. Therefore, alkyl chain-locked molecules have better intersystem crossing than that of 2-OMeDBF, which also led to shortened phosphorescence lifetime. The dihedral angles of these molecules affect their phosphorescence performance. As the degree of electronic exchange between two dibenzofurans in the axial skeleton was increased, the coupling from n orbitals of oxygen on the alkoxy groups to the delocalized π orbitals became significant, which promoted the intersystem crossing following the El-Sayed rule[65]. Hence, from (R/S)-OMe with the largest dihedral angle to (R)-1C with the smallest one, the ratio of phosphorescence to fluorescence was increased, and the lifetime of phosphorescence was decreased, suggesting boosted intersystem crossing. The evidence demonstrated that changes in molecular dihedral angles could alter the degree of conjugation and the ability of intersystem crossing. Besides, the shortening of chain length also increases the rigidity of the molecule. As a result, quantum yields of these molecules in solutions increase accordingly, from 17.6% of unlocked (R/S)-OMe to 18.4% of (R)-4C, to 20.3% of (R)-3C, and finally to 23.7% of (R)-1C, indicating that molecular rigidity restricts the dynamic molecular motions, thereby suppressing intrinsic nonradiative decays (Table S7).

Then, the chiroptical properties of these molecules were studied by circular dichroism (CD) and CPL spectrometry, which describes the chiral characteristics in the ground state[66] and excited state, respectively. The magnitude is evaluated by the dissymmetry factors of g_{abs} and g_{lum}, which are defined as $g_{abs} = \Delta\varepsilon/\varepsilon$ and $g_{lum} = 2\times(I_L-I_R)/(I_L+I_R)$, respectively, where $\Delta\varepsilon$ represents the absorption difference of the molar extinction coefficient of left and right circularly polarized light, I_L and I_R indicate the PL intensity of Left-CPL and Right-CPL. From the CD spectra in Figure 2b and Figure S3,

an obvious alternating positive and negative Cotton effect from 260 to 360 nm was observed, which matches well with the absorption bands in the 2-MeTHF solution and the chiral molecular configuration. Besides, the perfect mirrored imaging of (S)-1C and (R)-1C was found. CD can partially reflect molecular rigidity, i.e., the most rigid (R)-1C exhibited the strongest CD among coupled molecules. In detail, $|g_{abs}|$ of (R)-1C was up to 6.3×10^{-3}, and those of other molecules were between 5.3×10^{-3} and 5.7×10^{-3} (Table 1). Therefore, when the chain length of the locking ring was decreased gradually, the rigidity was increased, which was conducive to stabilizing the chiral structure at the ground state.

Generally, rigidity exerted a more pronounced effect on emission than on absorption since the excited state was more sensitive to the rigidity of the molecule.[67] To investigate the influence of molecular rigidity on the excited state, CPL measurements were conducted. As shown in Figure 3a, CPL spectra (Middle) coincided with the profile of overall PL spectra (Top). (R)-1C exhibited the strongest CPL intensity, followed by (R)-2C, (R)-3C, and (R)-4C, which was in line with their order of rigidity rather than their order of conjugation. Typically, CPL magnitude was evaluated by dissymmetry factor g_{lum}, and larger $|g_{lum}|$ was associated with better CPL characteristics. Considering the different overall PL intensity, we adopted individual g_{lum} to evaluate their CPL performance (Figure 3a Bottom). (R)-4C with flexible molecular structure exhibited a dissymmetry factor up to 8.4×10^{-4}. As the molecular rigidity was increased by shortened alkyl chain linker, the dissymmetry was increased. (R)-1C, with the most rigid molecular structure, exhibited the highest dissymmetry factor of 2.1×10^{-3}, which was about 2.5 folds that of (R)-4C (Table 1). Compared with $|g_{abs}|_{(R)\text{-}1C}/|g_{abs}|_{(R)\text{-}4C}$ (1.2), $|g_{lum}|_{(R)\text{-}1C}/|g_{lum}|_{(R)\text{-}4C}$ (2.5) was significantly larger, in agreement with that the molecular rigidity exerted a greater effect on the excited state. For comparison, the CPL of (S)-1C was also measured, which presented a mirror CPL with a dissymmetry factor $|g_{lum}|$ of up to 1.5×10^{-3}. The slight difference in $|g_{lum}|$ between (R)-1C and (S)-1C might be ascribed to the higher *ee* value in (R)-1C (Scheme 2). These results demonstrated that strong intramolecular rigidity boosted CPL.

As lowering temperature was one of the most effective ways to reduce molecular motions in the surrounding[68], we examined the influence of molecular motion on CPL by placing the solutions in a cryogenic condition. The temperature was maintained at 163 K to avoid false CPL signals caused by anisotropy during solvent crystallization. At low temperature, the emission wavelengths were redshifted. For instance, the emission

peak of (R)-2C was shifted from 348 nm to 355 nm, indicating that its dihedral angle was further decreased at low temperature (Figure 3 Top). As expected, all these molecules exhibited significant CPL enhancements. Especially, $|g_{lum}|$ was increased by several folds compared to that at room temperature (Figure 3 Bottom). The largest increase of $|g_{lum}|$ was determined from (R)-2C, which was increased from 1.0×10^{-3} at room temperature to 3.6×10^{-3} at 163 K by an amplification factor of 3.6. Among them, the largest $|g_{lum}|$ was obtained from (R)-1C, which was also amplified by 2.4 times compared to that at room temperature. These results demonstrated that low temperature reduced molecular motions and was also an effective way to promote CPL.

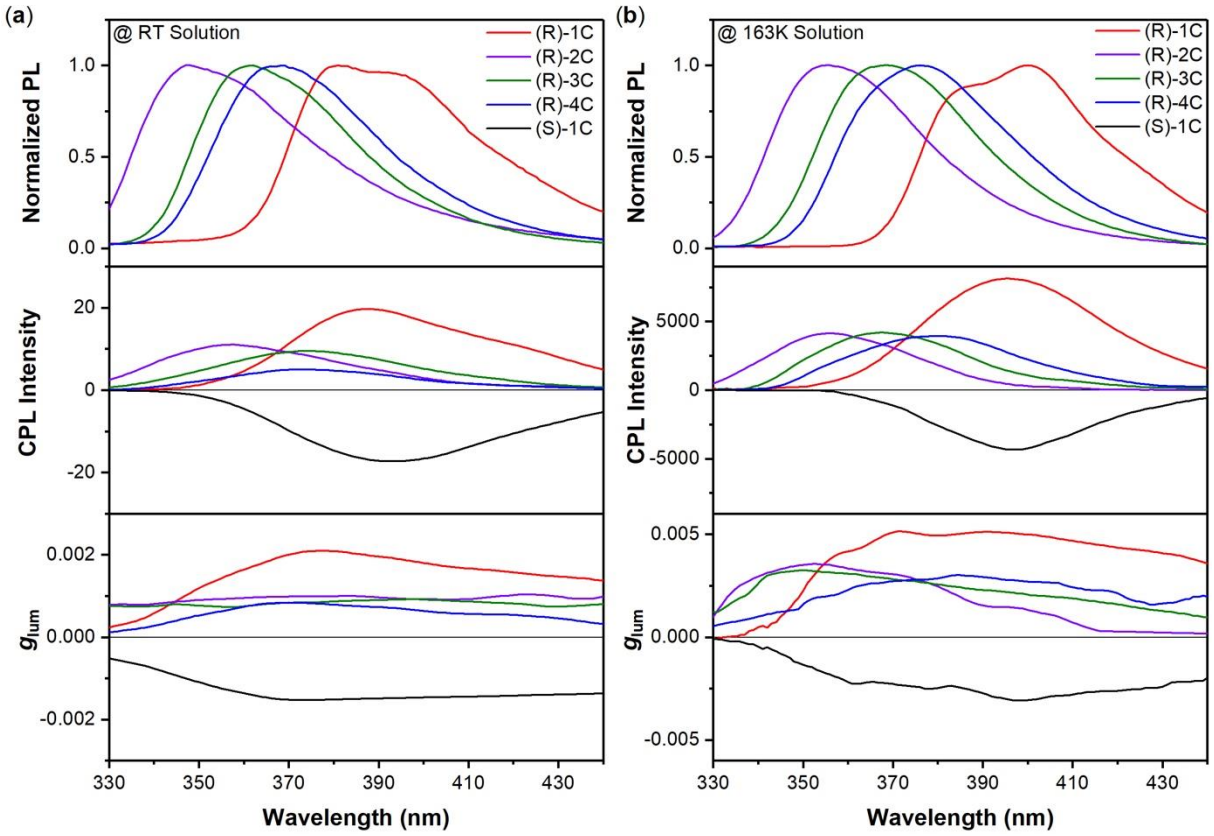

Figure 3. Normalized photoluminescence spectra (Top), CPL spectra (Middle), emissive dissymmetry factor g_{lum} (Bottom) of (R)-1C, (R)-2C, (R)-3C, (R)-4C and (S)-1C at (a) room temperature and (b) 163 K in 2-methyltetrahydrofuran (10^{-5} M).

To further explore the potential of CPL enhancement by restricting molecular motions, we measured the CPL of (R)-1C, (R)-2C, (R)-3C, (R)-4C, and (S)-1C crystals, in the hope of confining the scaffolds by the abundant intermolecular interactions in crystalline packing. As shown in Figure 4a and Table 1, these crystals presented rigidity-dependent CPL intensity in the crystal system with larger $|g_{lum}|$ values than those in solutions at room temperature. As the alkyl chain was shortened from 4C to 1C, the $|g_{lum}|$ was increased from 1.0×10^{-3} to 4.2×10^{-3} gradually. Compared with the solution state, the

amplitude of $|g_{lum}|_{(R\text{-}1C)}/|g_{lum}|_{(R\text{-}4C)}$ was significantly larger than that in the solution, which should be attributed to the synergetic effect of increased intramolecular rigidity and environmental confinements (Table 1). Besides, the CPL of (R)-2C was redshifted by 27 nm compared with its solution, suggestive of its decreased dihedral angle in crystals. (S)-1C demonstrated mirror-symmetric CPL with respective to (R)-1C, but the $|g_{lum}|$ of (S)-1C was slightly smaller due to its smaller *ee*. The above results demonstrated that multiple strategies of restriction of molecular motions could be adopted together for boosting CPL performance.

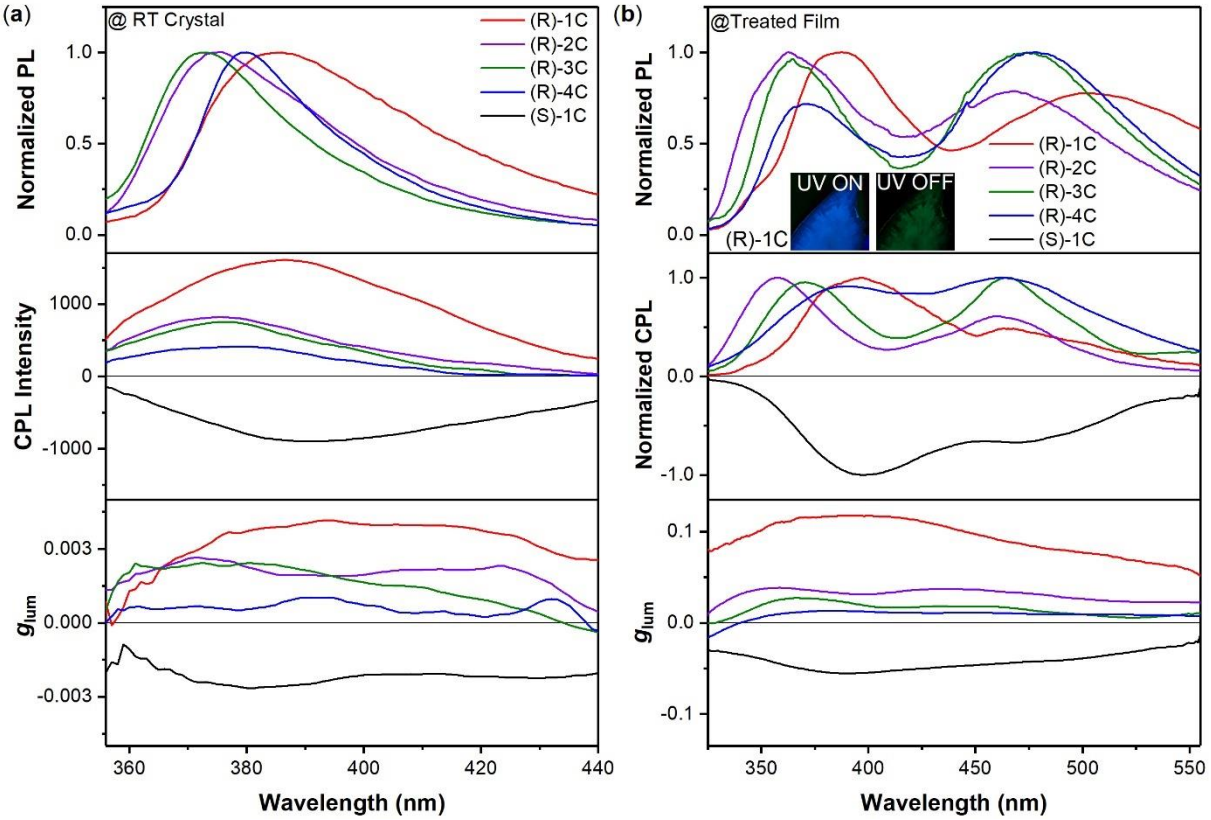

Figure 4. Normalized photoluminescence spectra (Top), CPL spectra (Middle), emissive dissymmetry factor g_{lum} (Bottom) of (R)-1C, (R)-2C, (R)-3C, (R)-4C and (S)-1C (a) crystals and (b) treated PVA films at room temperature. Inset: microscope photographs of treated film with doping (R)-1C taken before and after removal of the UV excitation source of 365 nm under ambient conditions.

Considering that the improvement in CPL was not remarkable in crystals, choosing a rigid and confinement matrix may offer a more powerful restriction of molecular motions. Poly(vinyl alcohol) (PVA) was recently selected as an ideal host matrix for constructing luminescent films owing to its abundant hydroxyl groups restricting both intermolecular and intramolecular motions via hydrogen bonding and its high crystallinity. Here, we prepared transparent PVA films at an optimized doping

concentration of 1:600 for the guest-host mass ratio. Upon thermal annealing and photoactivation, these PVA films underwent thermal crystallization and chain crosslinking to achieve enhanced rigidity and dense molecular interactions. A series of treated PVA films with doping (R)-1C, (R)-2C, (R)-3C, (R)-4C, and (S)-1C, respectively, were prepared. When subjected to visual observations and PL spectrometry characterizations (Figure 4b), these films exhibited intense luminescence under UV excitation and long afterglow after turning off the UV lamp (Figure 4b Inset for (R)-1C film). In PL spectra, there were dual emissions from singlet and triplet excited states, which corresponded to fluorescence (320-420 nm) and phosphorescence (420-650 nm) emission, respectively. Their luminescent nature was distinguished by their unimolecular decay lifetime profiles at 77 K (Figure S4 and Table S7). In comparison with solutions at 77 K, the emission wavelength did not change (Figure 4b and S4) because the PVA film matrix hosted the dye in the molecular state and did not alter their conformations, where giving the longest fluorescence and phosphorescence wavelength of (R)-1C, and the shortest one of (R)-2C. Thanks to the protective effect from the matrix, the triplet excitons were isolated from air and moisture, resulting in bright phosphorescence. These PVA films showed moderate quantum yields (9.2%-21.4%) and impressive persistent lifetimes up to 1438 ms (Table S7), which was attributed to the highly rigid intramolecular and intermolecular frameworks, pure $^3(\pi, \pi^*)$ character, and efficient intersystem crossing.

Table 1. The summaries of $|g_{lum}|$[a)] and $|g_{abs}|$[b)] of (R)-nC at different states.

$\|g\|$	(R)-1C	(R)-2C	(R)-3C	(R)-4C
$\|g_{sol\text{-}RT}\|$[a)]	2.1×10^{-3}	1.0×10^{-3}	9.2×10^{-4}	8.4×10^{-4}
$\|g_{sol\text{-}163K}\|$[a)]	5.1×10^{-3}	3.6×10^{-3}	3.2×10^{-3}	3.0×10^{-3}
$\|g_{cry}\|$[a)]	4.2×10^{-3}	2.6×10^{-3}	2.4×10^{-3}	1.0×10^{-3}
$\|g_{film}\|$[a)]	1.2×10^{-1}	3.8×10^{-2}	2.7×10^{-2}	1.3×10^{-2}
$\|g_{sol\text{-}RT}\|$[b)]	6.3×10^{-3}	5.3×10^{-3}	5.7×10^{-3}	5.3×10^{-3}

[a)] represents $|g_{lum}|$. [b)] represents $|g_{abs}|$.

To examine the effect of the PVA matrix on the chiroptical properties, we measured the CPL and $|g_{lum}|$ of treated films. For avoiding to collect false signals induced by linear polarized photoluminescence, the excitation-emission optical path adopts 90° reflection measurement in the CPL measuring module of Edinburgh Instruments FLS1000[16]. Compared with the solution state, these films exhibited enhanced CPL, especially $|g_{lum}|$ was increased by several dozens of folds (Figure 4b). For example, the $|g_{lum}|$ of (R)-4C film with the weakest CPL increased 15 folds, and that of (R)-1C film with the strongest

CPL increased 57 folds, which makes $|g_{lum}|$ up to 0.013 for (R)-4C and 0.12 for (R)-1C, respectively (Table 1). The order of these $|g_{lum}|$ was in accordance with the order of their molecular structure rigidity, which was demonstrative of the crucial role of rigidity in CPL performance. Excitingly, these samples exhibited attractive circularly polarized phosphorescence, with $|g_{lum}|$ values covering from 0.010 of (R)-4C film to 0.075 of (R)-1C film (Figure 4b Bottom). Collectively, strong molecular rigidity and great environmental confinement were essential factors for improving CPL performance due to the reduction of nonradiative relaxation pathways.

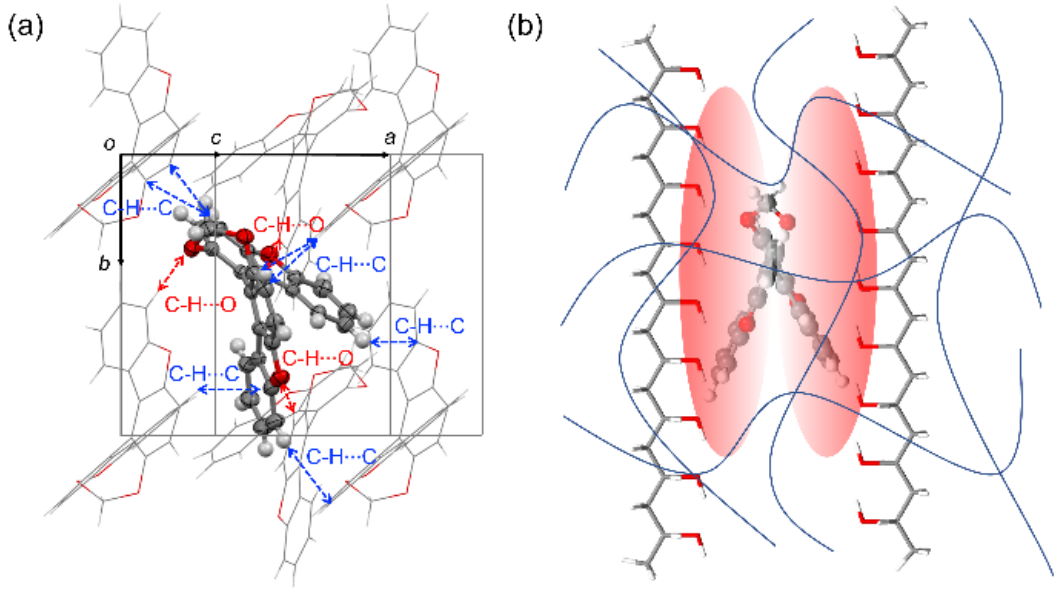

Figure 5. (a) Found Intermolecular interactions between adjacent molecules in crystal packing of (R)-1C. Selected central molecule is shown in ellipsoid mode and all interacted surrounding molecules are shown in wireframe mode. (b) Proposed intermolecular interactions between the dye molecules and PVA polymer chains.

Since environmental confinements induce remarkable enhancements of CPL from solution to crystal and to PVA film, from room-temperature to cryogenic condition, here, we intend to decipher these possible external effects. When dyes are dissolved in solution, the solvent molecules collide with the solvate dynamically. Multiple but weakly bundled interactions cannot stabilize the intrinsic intramolecular motions, especially when they are at excited states. As a result, dye in solutions often shows the poorest CPL performance. Here, upon alkylation of axial chiral scaffold, we finely increased the molecular rigidity by locking the twisting. The direct effect reduces the intramolecular vibrations and rotations, contributing to stabilizing dynamic excited states. Thus, it caused positive optical property changes of the improved molar extinction coefficient of

absorption, redshifted wavelength, and enhanced CPL emission, following the deduced dihedral angle from different chain lengths. However, the locking extent is limited, especially on flexible and rotatable axial chiral structure when dispersed in a dilute solution at room temperature. The temperature effect was then considered. The glass state is often applied to inhibit dynamic molecular motions to eliminate the intermolecular quenching factors, as the dye and solvent molecules are located at their positions. It was observed that the luminescent intensity and CPL emission were both increased at low temperature. These experimental results indicate that restriction of intramolecular and intermolecular motions was an effective way to improve chiroptical properties. Afterward, we scrutinize single-crystal structures and discover the probable intermolecular interactions which help to restrict molecular motions (Figure 5a). Multiple intermolecular weak hydrogen bonds and no π-π stacking were observed between adjacent molecules in the crystals. Especially, numbers of C-H…π, C-H…O, and C-H…C bonds were found, which effectively restrict molecular rotation and twisting. Among these interactions, C-H…O bonds have the shortest distance of 2.459 Å, indicating weak hydrogen bonds accounting for main intermolecular interactions. However, the determined packing mode requires the molecules to be located at specific positions, and thus only suitable interactions are allowed to construct the 3D crystal packing. So, multiple yet not adequate intermolecular interactions result in weakly enhanced CPL.

Finally, it is well known that PVA networks can be crosslinked by photo-induced reactions, thermal hardening, formaldehyde, or chemical reactions. Therefore, treated PVA networks provide sufficient intermolecular interactions, including strong hydrogen bonding, electrostatic, and dispersion interactions.[69] Particularly, the soft polymer chains and repeating hydroxyl groups can closely surround the molecularly dispersed dyes, giving superior restriction of molecular motions than crystal packing. Here, Fourier transform infrared spectroscopy was utilized to analyse existing molecular interactions (Figure S6)[70]. Abundant ν_{OH} at 3304 cm^{-1} revealed that overwhelming -OH groups in the PVA chain can provide sufficient hydrogen bonding with the oxygen and even more hydrogen atoms of doping molecules. Adequate vibrational bands around 1732 cm^{-1} and 1244 cm^{-1} were caused by photoactivation and interchain crosslinking for constructing the networks and inhibiting molecular motions. Furthermore, after thermal annealing, the edge surface of the PVA film achieved partial crystallization, as revealed by angle-dependent polarizing optical microscopy (Figure S7)[6]. The treated PVA films with

doping chiral molecules formed strong intramolecular and intermolecular interactions to inhibit intrinsic motions.

Together with their superior $|g_{lum}|$ of circularly polarized emission, we draw a solid structure-property relationship that restriction of molecular motion was a fascinating and effective method for achieving high-performance circularly polarized luminescence in small organic molecules. The excellent CPL performance is attributed to the large intramolecular rigidity and strong environmental restrictions on the alkyl-locked axis chiral scaffold. Experimental results confirm that they play the synergy effects in the restriction of molecular motions. When chiral molecules with flexible structures in unconfined conditions can only stem weak CPL due to inevitable motions. With increasing intramolecular rigidity and developing environmental confinements, greatly enhanced CPL can be achieved. Meanwhile, interesting circularly polarized phosphorescence can be generated when triplet excitons are isolated and protected by the strengthening-constrained environment.

3. Conclusions

In summary, we detailly investigated the structure-property relationship on a newly-developed axial chiral scaffold of bidibenzo[*b*,*d*]furan. Through finely tuning the molecular rigidity by gradually reducing the alkyl-chain length and varying the environmental confinement factors in solution, crystal, and polymer-matrix at different temperatures, we found the general rule that the restriction of molecular motions plays the positive impact on boosting circularly polarized luminescence. They exert the synergistic effect by integrating intramolecular rigidification and sufficient intermolecular interactions to stabilize the chiral excited configurations and deduce the nonradiative decay pathways. As a result, a significant amplification of the dissymmetry factor from 10^{-4} to 10^{-1} with a 146-fold magnification was achieved. The clear and positive relationship was carefully demonstrated on the flexible and chiral axial scaffold. Unfortunately, further improving circularly polarized luminescence with a larger g_{lum} was not obtained, which led us to discover better restriction conditions in our lab. Nevertheless, our work not only provided a deeper insight into the structure-property relationship but also proposed an effective strategy of boosting the circularly polarized luminescence of small organic molecules, which will be of great importance for developing high-performance small organic chiroptical systems in the future.

Acknowledgements

This work was supported by the National Natural Science Foundation of China (21975061), the Shenzhen Fundamental Research Program (GXWD20201230155427003-20200728150952003, JCYJ20190806142403535).

Author Contributions

The design and experimental guidance of the project were completed by Prof. Dr. Zikai He. The exploration of experiments and the characterization of materials were completed by Mr. Wenbin Huang. Single-crystal characterization and refinement were completed by Dr. Kang Zhou. The manuscript was edited by Prof. Dr. Engui Zhao.

Conflicts of Interest

The authors declare no conflicts of interest.

Received: ((will be filled in by the editorial staff))

Revised: ((will be filled in by the editorial staff))

Published online: ((will be filled in by the editorial staff))

References

[1] J. R. Brandt, F. Salerno, M. J. Fuchter, *Nat. Rev. Chem.* **2017**, 1, 0045.
[2] Z. Jiang, J. Wang, T. Gao, J. Ma, Z. Liu, R. Chen, *ACS Appl. Mater. Interfaces* **2020**, 12, 9520-9527.
[3] G. Yang, Z. Yao, X. Yang, Y. Xie, P. Duan, Y. M. Zhang, S. X.-A. Zhang, *Adv. Sci.* **2022**, 9, e2202636.
[4] C. Zhang, S. Li, X. Dong, S. Zang, *Aggregate* **2021**, 2, e48.
[5] H. Li, H. Li, W. Wang, Y. Tao, S. Wang, Q. Yang, Y. Jiang, C. Zheng, W. Huang, R. Chen, *Angew. Chem. Int. Ed.* **2020**, 59, 4756-4762.
[6] W. Huang, C. Fu, Z. Liang, K. Zhou, Z. He, *Angew. Chem. Int. Ed.* **2022**, 61, e202202977.
[7] M. Louis, R. Sethy, J. Kumar, S. Katao, R. Guillot, T. Nakashima, C. Allain, T. Kawai, R. Metivier, *Chem. Sci.* **2019**, 10, 843-847.
[8] X. Song, X. Zhu, S. Qiu, W. Tian, M. Liu, *Angew. Chem. Int. Ed.* **2022**, 61, e202208574.
[9] Y. He, S. Zhang, H. K. Bisoyi, J. Qiao, H. Chen, J. Gao, J. Guo, Q. Li, *Angew. Chem. Int. Ed.* **2021**, 60, 27158-27163.
[10] L. Frédéric, A. Desmarchelier, L. Favereau, G. Pieters, *Adv. Funct. Mater.* **2021**, 31, 2010281.
[11] X. Wu, J. W. Huang, B. K. Su, S. Wang, L. Yuan, W. Q. Zheng, H. Zhang, Y. X. Zheng, W. Zhu, P. T. Chou, *Adv. Mater.* **2022**, 34, e2105080.
[12] R. Liu, B. Ding, D. Liu, X. Ma, *Chem. Eng. J.* **2021**, 421, 129732.
[13] L. Gu, W. Ye, X. Liang, A. Lv, H. Ma, M. Singh, W. Jia, Z. Shen, Y. Guo, Y. Gao, H. Chen, D. Wang, Y. Wu, J. Liu, H. Wang, Y. X. Zheng, Z. An, W. Huang, Y. Zhao, *J. Am. Chem. Soc.* **2021**, 143, 18527-18535.
[14] S. Hirata, M. Vacha, *J. Phys. Chem. Lett.* **2016**, 7, 1539-1545.
[15] S. Garain, S. Sarkar, B. Chandra Garain, S. K. Pati, S. J. George, *Angew. Chem. Int. Ed.* **2022**, 61, e202115773.
[16] W. Chen, Z. Tian, Y. Li, Y. Jiang, M. Liu, P. Duan, *Chem. - Eur. J.* **2018**, 24, 17444-17448.
[17] Z. Huang, Z. He, B. Ding, H. Tian, X. Ma, *Nat. Commun.* **2022**, 13, 7841.

[18] C. Xue, L. Xu, H. X. Wang, T. Li, M. Liu, *ChemPhotoChem* **2022**, 6, e202100255.
[19] K. Takaishi, K. Iwachido, T. Ema, *J. Am. Chem. Soc.* **2020**, 142, 1774-1779.
[20] Q. Ye, F. Zheng, E. Zhang, H. K. Bisoyi, S. Zheng, D. Zhu, Q. Lu, H. Zhang, Q. Li, *Chem. Sci.* **2020**, 11, 9989-9993.
[21] G. Ouyang, J. Ruhe, Y. Zhang, M. J. Lin, M. Liu, F. Wurthner, *Angew. Chem. Int. Ed.* **2022**, 61, e202206706.
[22] M. Hu, F. Y. Ye, C. Du, W. Wang, T. T. Zhou, M. L. Gao, M. Liu, Y. S. Zheng, *ACS nano* **2021**, 15, 16673-16682.
[23] L. Cui, H. Shinjo, T. Ichiki, K. Deyama, T. Harada, K. Ishibashi, T. Ehara, K. Miyata, K. Onda, Y. Hisaeda, T. Ono, *Angew. Chem. Int. Ed.* **2022**, 61, e202204358.
[24] Z. Q. Li, Z. L. Gong, J. Y. Shao, J. Yao, Y. W. Zhong, *Angew. Chem. Int. Ed.* **2021**, 60, 14595-14600.
[25] Z. Liu, J. Ren, P. Li, L. Niu, Q. Liao, S. Zhang, Q. Yang, *Angew. Chem. Int. Ed.* **2022**, Accepted, DOI: 10.1002/anie.202214211.
[26] J. Han, Y. Shi, X. Jin, X. Yang, P. Duan, *Chem. Sci.* **2022**, 13, 6074-6080.
[27] X. Pan, A. Zheng, X. Yu, Q. Di, L. Li, P. Duan, K. Ye, P. Naumov, H. Zhang, *Angew. Chem. Int. Ed.* **2022**, 61, e202203938.
[28] J. Hou, R. Toyoda, S. C. J. Meskers, B. L. Feringa, *Angew. Chem. Int. Ed.* **2022**, 61, e202206310.
[29] D. Han, C. Li, C. Jiang, X. Jin, X. Wang, R. Chen, J. Cheng, P. Duan, *Aggregate* **2021**, 3, e148.
[30] X. Zhang, Y. Xu, C. Valenzuela, X. Zhang, L. Wang, W. Feng, Q. Li, *Light: Sci. Appl.* **2022**, 11, 223.
[31] E. S. Gauthier, L. Abella, N. Hellou, B. Darquie, E. Caytan, T. Roisnel, N. Vanthuyne, L. Favereau, M. Srebro-Hooper, J. A. G. Williams, J. Autschbach, J. Crassous, *Angew. Chem. Int. Ed.* **2020**, 59, 8394-8400.
[32] K. Harada, R. Sekiya, T. Haino, *Angew. Chem. Int. Ed.* **2022**, 61, e202209340.
[33] H. Li, B. S. Li, B. Z. Tang, *Chem. - Asian J.* **2019**, 14, 674-688.
[34] S. Zheng, J. Han, X. Jin, Q. Ye, J. Zhou, P. Duan, M. Liu, *Angew. Chem. Int. Ed.* **2021**, 60, 22711-22716.
[35] J. Wade, J. R. Brandt, D. Reger, F. Zinna, K. Y. Amsharov, N. Jux, D. L. Andrews, M. J. Fuchter, *Angew. Chem. Int. Ed.* **2021**, 60, 222-227.
[36] C. Maeda, K. Nagahata, T. Shirakawa, T. Ema, *Angew. Chem. Int. Ed.* **2020**, 59, 7813-7817.
[37] K. Takaishi, T. Matsumoto, M. Kawataka, T. Ema, *Angew. Chem. Int. Ed.* **2021**, 60, 9968-9972.
[38] H. Shigemitsu, K. Kawakami, Y. Nagata, R. Kajiwara, S. Yamada, T. Mori, T. Kida, *Angew. Chem. Int. Ed.* **2022**, 61, e202114700.
[39] Z. Qiu, C. W. Ju, L. Frederic, Y. Hu, D. Schollmeyer, G. Pieters, K. Mullen, A. Narita, *J. Am. Chem. Soc.* **2021**, 143, 4661-4667.
[40] K. Watanabe, K. Akagi, *Sci. Technol. Adv. Mater.* **2014**, 15, 044203.
[41] Y. Deng, M. Wang, Y. Zhuang, S. Liu, W. Huang, Q. Zhao, *Light: Sci. Appl.* **2021**, 10, 76.
[42] M. Morgenroth, M. Scholz, L. Guy, K. Oum, T. Lenzer, *Angew. Chem. Int. Ed.* **2022**, 61, e202203075.
[43] X. Yang, X. Jin, T. Zhao, P. Duan, *Mater. Chem. Front.* **2021**, 5, 4821-4832.
[44] Y. Wu, C. Yan, X. S. Li, L. H. You, Z. Q. Yu, X. Wu, Z. Zheng, G. Liu, Z. Guo, H. Tian, W. H. Zhu, *Angew. Chem. Int. Ed.* **2021**, 60, 24549-24557.
[45] J. Liu, Y. Molard, M. E. Prevot, T. Hegmann, *ACS Appl. Mater. Interfaces* **2022**, 14, 29398-29411.

[46] J. Mei, N. L. C. Leung, R. T. K. Kwok, J. W. Y. Lam, B. Z. Tang, *Chem. Rev.* **2015**, 115, 11718-11940.
[47] S. K. Keshri, A. Takai, T. Ishizuka, T. Kojima, M. Takeuchi, *Angew. Chem. Int. Ed.* **2020**, 59, 5254-5258.
[48] Y. Nojima, M. Hasegawa, N. Hara, Y. Imai, Y. Mazaki, *Chem. - Eur. J.* **2021**, 27, 5923-5929.
[49] N. Zhao, W. Gao, M. Zhang, J. Yang, X. Zheng, Y. Li, R. Cui, W. Yin, N. Li, *Mater. Chem. Front.* **2019**, 3, 1613-1618.
[50] H. Zhang, H. Li, J. Wang, J. Sun, A. Qin, B. Z. Tang, *J. Mater. Chem. C* **2015**, 3, 5162-5166.
[51] S. Hu, L. Hu, X. Zhu, Y. Wang, M. Liu, *Angew. Chem. Int. Ed.* **2021**, 60, 19451-19457.
[52] Z. Li, Y. Han, F. Nie, M. Liu, H. Zhong, F. Wang, *Angew. Chem. Int. Ed.* **2021**, 60, 8212-8219.
[53] J. B. Xiong, H. T. Feng, J. P. Sun, W. Z. Xie, D. Yang, M. Liu, Y. S. Zheng, *J. Am. Chem. Soc.* **2016**, 138, 11469-11472.
[54] M. Hu, F. Y. Ye, C. Du, W. Wang, W. Yu, M. Liu, Y. S. Zheng, *Angew. Chem. Int. Ed.* **2022**, 61, e202115216.
[55] K. Takaishi, S. Murakami, F. Yoshinami, T. Ema, *Angew. Chem. Int. Ed.* **2022**, 61, e202204609.
[56] A. Mukherjee, D. S. Pal, H. Kar, S. Ghosh, *Polym. Chem.* **2020**, 11, 7481-7486.
[57] J. Liu, H. Su, L. Meng, Y. Zhao, C. Deng, J. C. Y. Ng, P. Lu, M. Faisal, J. W. Y. Lam, X. Huang, H. Wu, K. S. Wong, B. Z. Tang, *Chem. Sci.* **2012**, 3, 2737-2747.
[58] X. Wang, H. Guo, C. Yu, Y. Jing, Z. Han, X. Ma, C. Yang, M. Liu, D. Zhai, D. Zheng, Y. Pan, X. Li, K. Ding, *Macromolecules* **2021**, 54, 11180-11186.
[59] X. Tang, H. Jiang, Y. Si, N. Rampal, W. Gong, C. Cheng, X. Kang, D. Fairen-Jimenez, Y. Cui, Y. Liu, *Chem* **2021**, 7, 2771-2786.
[60] Y. Wang, D. Niu, G. Ouyang, M. Liu, *Nat. Commun.* **2022**, 13, 1710.
[61] A. E. S. Gelpke, J. Fraanje, K. Goubitz, H. Schenk, H. Hiemstra, *Tetrahedron* **1997**, 53, 5899-5908.
[62] S. Lu, S. B. Poh, Y. Zhao, *Angew. Chem. Int. Ed.* **2014**, 53, 11041-11045.
[63] Y. Geng, M. A. Ali, A. J. Clulow, S. Fan, P. L. Burn, I. R. Gentle, P. Meredith, P. E. Shaw, *Nat. Commun.* **2015**, 6, 8240.
[64] S. Suzuki, S. Sasaki, A. S. Sairi, R. Iwai, B. Z. Tang, G. I. Konishi, *Angew. Chem. Int. Ed.* **2020**, 59, 9856-9867.
[65] W. Zhao, Z. He, J. W. Y. Lam, Q. Peng, H. Ma, Z. Shuai, G. Bai, J. Hao, B. Z. Tang, *Chem* **2016**, 1, 592-602.
[66] N. Berova, L. Di Bari, G. Pescitelli, *Chem. Soc. Rev.* **2007**, 36, 914-931.
[67] Q. Peng, Y. Yi, Z. Shuai, J. Shao, *J. Am. Chem. Soc.* **2007**, 129, 9333-9339.
[68] Y. Kondo, S. Suzuki, M. Watanabe, A. Kaneta, P. Albertini, K. Nagamori, *Front. Chem.* **2020**, 8, 527.
[69] D. Wang, H. Wu, J. Gong, Y. Xiong, Q. Wu, Z. Zhao, L. Wang, D. Wang, B. Z. Tang, *Mater. Horiz.* **2022**, 9, 1081-1088.
[70] Y. Su, S. Z. F. Phua, Y. Li, X. Zhou, D. Jana, G. Liu, W. Q. Lim, W. K. Ong, C. Yang, Y. Zhao, *Sci. Adv.* **2018**, 4, eaas9732.